

# Electron trapping by neutral, pristine ferroelectric domain walls in $\text{BiFeO}_3$

Sabine Körbel

*School of Physics, AMBER and CRANN Institute, Trinity College, Dublin 2, Ireland and  
Institute of Physics, Academy of Sciences of the Czech Republic, Na Slovance 2, 182 21 Prague 8, Czech Republic*

Jirka Hlinka

*Institute of Physics, Academy of Sciences of the Czech Republic, Na Slovance 2, 182 21 Prague 8, Czech Republic*

Stefano Sanvitto

*School of Physics, AMBER and CRANN Institute, Trinity College, Dublin 2, Ireland*

First-principles calculations for pristine neutral ferroelectric domain walls in  $\text{BiFeO}_3$  reveal that excess electrons are selectively trapped by the domain walls, while holes are only weakly attracted. Such trapped excess electrons can be responsible for the thermally activated electrical conductivity at domain walls observed in experiments. In the case of a periodic array of domain walls, the trapped excess electrons create a zig-zag potential, whose amplitude depends on the electron concentration in the material and the domain-wall distance. The potential is asymmetric for  $71^\circ$  and  $109^\circ$  domain walls. This could increase the open-circuit voltage in a solar cell and hence be beneficial for the photoelectric effect in  $\text{BiFeO}_3$ .

PACS numbers:

## I. INTRODUCTION

The ferroelectric oxide  $\text{BiFeO}_3$  exhibits the photovoltaic effect, which makes it a prototype material to study ferroelectric photovoltaic. In principle, ferroelectric photovoltaics are promising materials for solar cells because their polar structure allows one to extract a photocurrent without the need to create a  $p - n$  junction by doping. In practice, ferroelectrics are usually large-band gap materials, with low light absorption in the visible range. Two quantities are important for an efficient solar-cell absorber: the photocurrent, and the photovoltage, both of which should ideally be large. Ferroelectrics can at least fulfil one of the two requirements, in that their open-circuit voltage can be very large. This feature has first been ascribed to ferroelectric domain walls (DWs) acting as a series of naturally occurring  $p - n$  junctions<sup>1</sup>. However, later experiments<sup>2</sup> and first-principles calculations of the bulk pho-

tovoltaic effect (BPVE) in  $\text{BiFeO}_3$ <sup>3</sup> show that the observed large photovoltage of  $\text{BiFeO}_3$  can be explained on the basis of the BPVE alone, with no need for DW contributions. This means that the rôle and function of DWs on the photovoltage is still not clear.

In Refs. [1] and [4] a model for the DW contribution to the photovoltage was proposed (see Fig 1), where discontinuities in the ferroelectric polarization at the DWs lead to electrostatic potential steps. These separate the photogenerated charges and trap electrons and holes at opposite sides of the DWs with an approximately symmetric distribution, thus impeding charge-carrier recombination by spatial separation. First-principles calculations using density-functional theory (DFT) were performed previously to investigate the electronic potential at DWs in  $\text{BiFeO}_3$ <sup>5-7</sup> using indirect methods to determine the potential at the DW and considering only systems without excess charge carriers.

Here we show that it is necessary to go beyond these approaches and to both calculate directly the electronic poten-

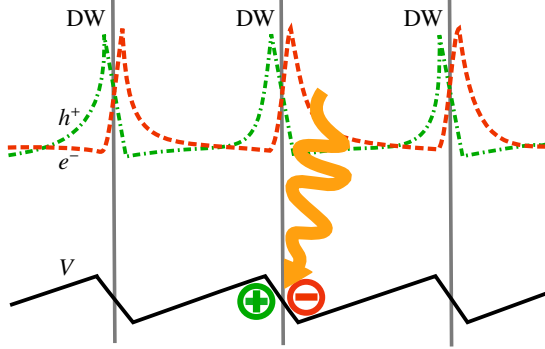


FIG. 1: (Color online) Previously proposed model for the charge-carrier distribution (upper panel) of excess electrons,  $e^-$  (orange dashed line), and holes,  $h^+$  (green dot-dashed line), and the electronic potential (lower panel),  $V$ , at domain walls. All curves are schematic.

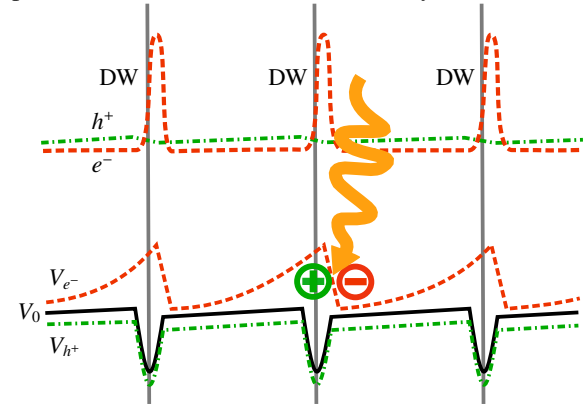


FIG. 2: (Color online) Our proposed model for charge-carrier distribution and electronic potential. In the lower panel we show the electronic potential without free charge carriers  $V_0$  (black solid line), and in the case of excess electrons  $V_{e^-}$  or holes  $V_{h^+}$ .

tial and take explicitly into account excess charges to reveal the unusual charge localization behavior and the nature of the electronic zig-zag potential in  $\text{BiFeO}_3$ . We find important deviations in the charge-density distribution and the electrostatic potential with respect to the previously proposed model: excess electrons are indeed trapped at the domain walls, but holes are strongly delocalized, leading to an asymmetric charge density distribution. As a consequence the potential has indeed a zig-zag profile, but this largely originates from the trapped excess electrons. The previously proposed model is depicted in Fig. 1, and our suggested modification is in Fig. 2.

## II. METHODS

In rhombohedral perovskites, such as  $\text{BiFeO}_3$ , the polarization in adjacent domains can form angles of about  $71^\circ$ ,  $109^\circ$ , and  $180^\circ$ , which are all studied here. For each DW angle, we selected the DW with the lowest possible Miller indices which is electrically neutral and mechanically compatible.<sup>8</sup> First-principles DFT calculations were performed with the `vasp` code<sup>9</sup>, using the Projector-Augmented Wave (PAW) method and pseudopotentials with 5 (Bi), 16 (Fe), and 6 (O) valence electrons, respectively. We used the local-density approximation (LDA), and corrected the band gap with a Hubbard- $U$  term of 5.3 eV following Dudarev's scheme.<sup>10</sup> This  $U$  value was taken from the materials project<sup>11</sup> and it is optimized for oxide formation energies, but also yields band gaps close to experiments. The reciprocal space was sampled with  $2 \times 5 \times 3$   $k$ -points for the  $71^\circ$  and  $180^\circ$  DW, and with  $2 \times 5 \times 5$   $k$ -points for the  $109^\circ$  wall. Plane-wave basis functions with energies up to 520 eV were used. We employed a supercell approach with periodic boundary conditions, such that each supercell contains 120 atoms and two domain walls. Both the atomic positions and cell parameters were allowed to relax until the energy difference between ionic relaxation steps fell below 0.1 meV. We use a coordinate system with axes  $\{\mathbf{e}_r, \mathbf{e}_s, \mathbf{e}_t\}$ , where  $\mathbf{e}_r \parallel P_r$  is the polarization component which changes sign at the domain wall,  $\mathbf{e}_s$  is perpendicular to the domain-wall plane, and  $\mathbf{e}_t = \mathbf{e}_r \times \mathbf{e}_s$ . The polarization profiles were calculated from the ionic positions  $\mathbf{u}_i$  and the formal ionic charges,  $Z_i$  ( $\text{Bi}^{3+}$ ,  $\text{Fe}^{3+}$  and  $\text{O}^{2-}$ ), weighted by  $w_i$  ( $w_{\text{Bi}} = 1/8$ ;  $w_{\text{Fe}} = 1$ ; and  $w_{\text{O}} = 1/2$ ) for each 5-atom perovskite cell as

$$\mathbf{P} = \sum_i w_i Z_i^* \mathbf{u}_i. \quad (1)$$

In order to investigate the localization of the excess charges, we calculated their densities as

$$\varrho_{\text{excess}} = \begin{cases} \sum_{ck} |\psi_{ck}|^2 f_{ck} & (\text{electrons}) \\ \sum_{vk} |\psi_{vk}|^2 (1 - f_{vk}) & (\text{holes}), \end{cases} \quad (2)$$

where  $f_{vk}$  is the occupation number of the Bloch function  $\psi_{vk}$ , and  $v$  and  $c$  are the valence- and conduction-band indices, respectively.

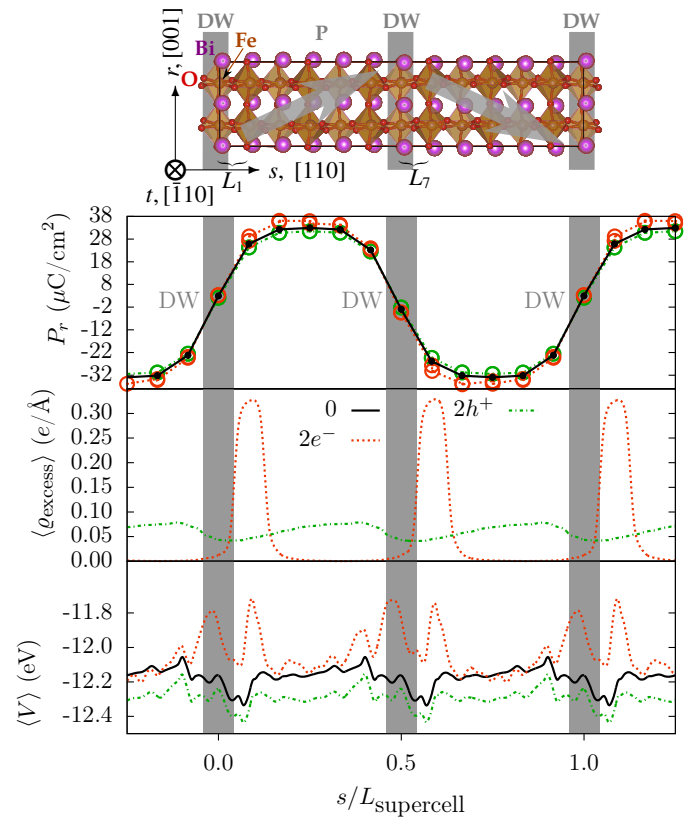


FIG. 3: (Color online) Characterisation of the  $71^\circ$  DW. Ferroelectric polarization profile  $P_r$  (top), charge density  $\varrho_{\text{excess}}$  of excess electrons and holes (center), and electronic potential  $V$  (bottom).  $P_r$  is the  $r$  component of the polarization.  $\varrho_{\text{excess}}$  and  $V$  are averaged over one atomic layer to smoothen strong rapid oscillations at atomic nuclei.<sup>12</sup> Results are presented for the neutral cell (solid black line), and for those containing two extra electrons,  $2e^-$  (dashed red line), or two extra holes,  $2h^+$  (dashed green line).

## III. RESULTS

In the top panels of figures 3, 4 and 5 we show the polarization profile,  $P_r$ , across the DW. This is the polarization component along the  $r$  direction, calculated from Eq. (1). Clearly for all DWs the polarization profile remains unchanged regardless of the cell's total charge (neutral, positively and negatively charged), meaning that the polar state of the DW structure is insensitive to charging.

In the center panels we show the excess charge density profile upon injection of holes or electrons (two charges per unit cell). In the case of electrons such additional charge localizes tightly at the DWs. In contrast the positive hole charge distributes over the entire cell. For the  $71^\circ$  DW one can still observe some moderate hole localization at the DW side opposite to that where the electrons accumulate, but this is absent for the  $109^\circ$  and  $180^\circ$  DWs, for which the holes are completely delocalized. The potential resulting from such charge distribution is presented next in the bottom panels (here we show the full Kohn-Sham potential). Let us focus first on that found for the neutral cell (solid black line). For the  $71^\circ$  and

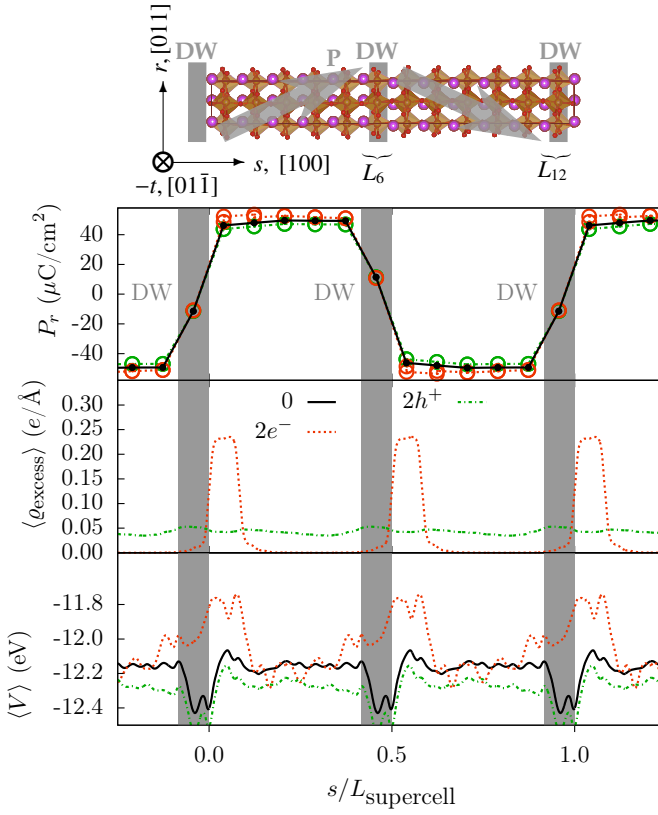


FIG. 4: (Color online) Characterisation of the 109° DW. Ferroelectric polarization profile  $P_r$  (top), charge density  $\varrho_{\text{excess}}$  of excess electrons and holes (center), and electronic potential  $V$  (bottom).  $P_r$  is the  $r$  component of the polarization. Results are presented for the neutral cell (solid black line), and for those presenting two extra electrons,  $2e^-$  (dashed orange line), or two extra holes,  $2h^+$  (dot-dashed green line).

109° DWs the dominant feature in the potential is a narrow local minimum, which extends over up to two perovskite monolayers at the domain wall. In the case of the 71° DW such potential minimum is superimposed over a less pronounced upward slope along the  $e_s$  direction (increasing when going from left to right in Fig. 3;  $\parallel P_s$ ). The same potential slope is not distinguishable for the 109° and 180° DWs, and in the latter case also the potential well disappears. Despite the differences in the potential among the three DWs excess charges distribute similarly, as described above. The charge accumulation in the case of excess electrons modifies the potential, which is now strongly repulsive at the DW (see dashed orange lines). In contrast, hole doping, where the positive charge distributes uniformly across the cell, affects little the general shape of the potential and its only effect is an approximately rigid energy shift (dashed green lines). Thus we conclude that in a situation of excess of electrons, which can arise from intentional doping, intrinsic defects or photo-carrier generation, the potential will present a zig-zag profile along the cell.

Our calculation has shown that it is possible to store about one electron per DW in our unit cell, which has a high DW density. This can be extrapolated to the more realistic condi-

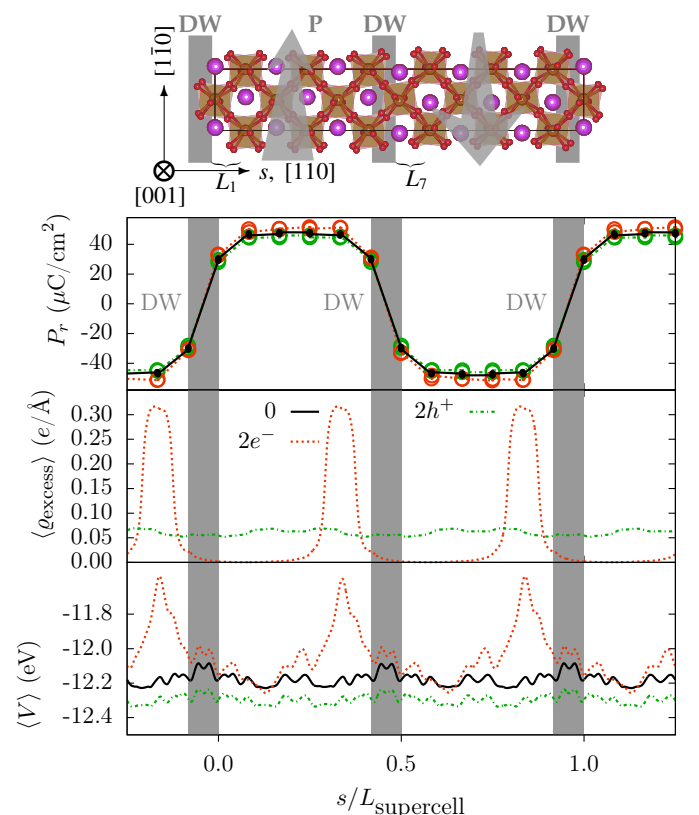


FIG. 5: (Color online) Characterisation of the 180° DW. Ferroelectric polarization profile  $P_r$  (top), charge density  $\varrho_{\text{excess}}$  of excess electrons and holes (center), and electronic potential  $V$  (bottom).  $P_r$  is the  $r$  component of the polarization. Here  $r \parallel [1\bar{1}0]$  and  $t \parallel [\bar{1}12]$ . Results are presented for the neutral cell (solid black line), and for those containing two extra electrons,  $2e^-$  (dashed orange line), or two extra holes,  $2h^+$  (dot-dashed green line).

tion met in experiments<sup>1</sup> in which the average DW spacing is about 140 nm. Such extrapolation returns us a situation where an electron density of at least  $10^{19} \text{ cm}^{-3}$  can be accommodated at the domain walls.

The effect of the DW and of the charge accumulation on the electronic structure is analysed next in Fig. 6, where we show the layer-resolved density of states (DOS) for the different charging situations investigated here. For both the neutral and the positively charged cells the DOS appears little perturbed by the presence of the DW, and it is essentially identical regardless of the layer on which it is projected. In contrast, when excess electrons are introduced, one can clearly observe the formation of two narrow peaks in the DOS localised at the layers adjacent to the DW. The gap level close to the valence band originates from occupied Fe  $d$  orbitals oriented along Fe-O bonds being pushed energetically upwards, while the one at higher energy is from the Fe  $d$  orbitals that are directed away from Fe-O bonds and are occupied by the excess electron. These electronic trap states might be experimentally detectable in photoemission experiments.

In both Ref. [2] and [4], the domain walls in BiFeO<sub>3</sub> were found to be more conductive than the domain interior. Such

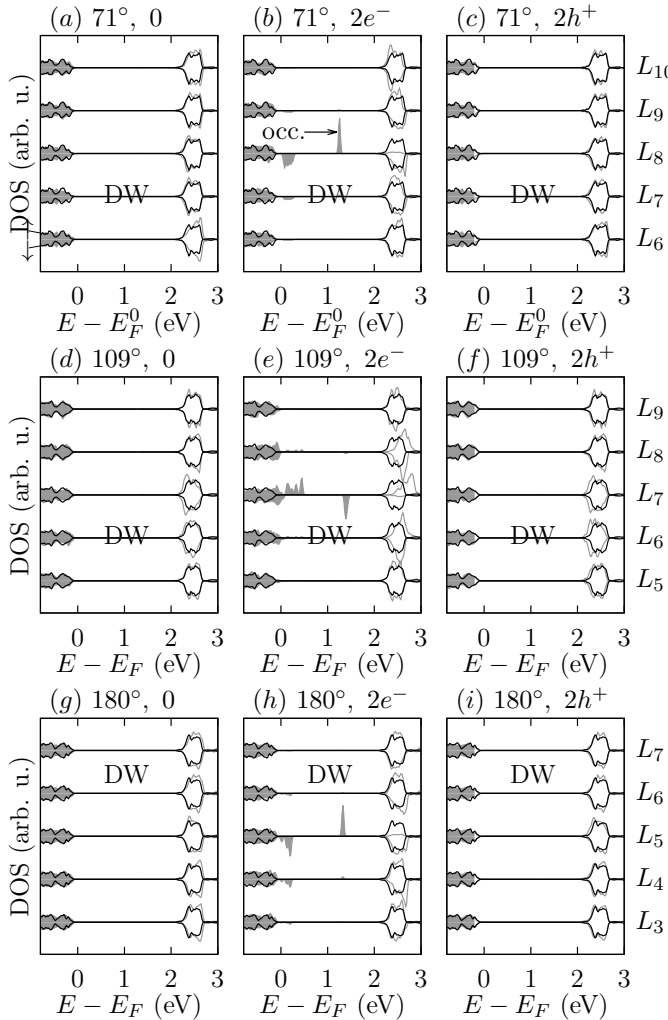


FIG. 6: Density of states (DOS) of the  $71^\circ$  domain-wall system (gray) and the monodomain system (black) projected on the atomic layers. (a) Domain wall without excess charges, (b) domain wall with electrons, (c) domain wall with holes. (d) to (f) are the same as (a) to (c) for the  $109^\circ$  domain wall, and (g) to (i) are the same for the  $180^\circ$  domain wall.  $E_F^0$  is the Fermi energy of the system without excess charges. Occupied levels are shaded in gray. The DOS for positive spin ( $\uparrow$ ) and negative spin ( $\downarrow$ ) are both shown, the  $\downarrow$ -DOS was multiplied by -1. DOS were vertically shifted for better visibility.

domain-wall conductivity appears to be thermally activated,<sup>2</sup> and trap states about 1 eV below the conduction band are involved in the photocurrent generation.<sup>13</sup> The deep levels which we find at electron-doped domain walls could provide such trap states. In this study we consider the idealised case of

pristine domain walls, which is well defined, but incomplete. Real samples contain various amounts of oxygen vacancies and/or other point defects, which may aggregate at the DWs. These may modify the electronic potential and the amount of excess electrons by acting as traps. Therefore a fully realistic picture will be obtained by considering pristine domain-wall sections, intersected by point defects. Notably, the presence of point defects at domain walls could also influence the resistivity of the walls themselves.

#### IV. SUMMARY AND CONCLUSION

Ferroelectric domain walls in  $\text{BiFeO}_3$  strongly trap excess electrons, but only weakly attract holes. The different localization behavior of electrons and holes at the walls may be understood on the basis of the electronic states which dominate the top of the valence band (delocalized O  $p$  states) and the bottom of the conduction band (localized Fe  $d$  states).

The potential profile at the domain walls is dominated by excess charge carriers. Without excess electrons, the electronic potential at the domain wall exhibits only a shallow zig-zag profile. Once electrons are trapped in the domain walls, the walls become repulsive for further electrons. This strongly repulsive potential created by the excess electrons trapped in the walls forms a strong zig-zag profile, whose amplitude depends on excess-electron and domain-wall density. In the case of the  $71^\circ$  and the  $109^\circ$  domain walls, the potential is asymmetric, which would enable a net photovoltaic current generation. In the case of the  $180^\circ$  domain wall, the potential is approximately symmetric, indicating that this wall may be photovoltaically less active. Based on these findings, we propose to modify the model for charge-carrier densities and potential at domain walls. The trap states for electrons at domain walls in  $\text{BiFeO}_3$  may be at the origin of the thermally activated domain-wall conduction found in experiments.

#### Acknowledgement

This project has received funding from the European Union's Horizon 2020 research and innovation programme under the Marie Skłodowska-Curie Grant Agreement No. 746964 - FERROVOLT and from the Czech Science Foundation (Project No. 15-04121S). Computation time and support provided by the Czech Metacentrum and the Trinity Centre for High Performance Computing funded by Science Foundation Ireland is gratefully acknowledged. Figures were made using gnuplot. Atomic structures were visualized with VESTA.<sup>14</sup>

<sup>1</sup> J. Seidel, D. Fu, S.-Y. Yang, E. Alarcón-Lladó, J. Wu, R. Ramesh, and J. W. Ager III, Physical review letters **107**, 126805 (2011).

<sup>2</sup> A. Bhatnagar, A. R. Chaudhuri, Y. H. Kim, D. Hesse, and M. Alexe, Nature Communications **4**, 2835 (2013).

<sup>3</sup> S. M. Young, F. Zheng, and A. M. Rappe, Phys. Rev. Lett. **109**,

236601 (2012).

<sup>4</sup> S. Y. Yang, J. Seidel, S. J. Byrnes, P. Shafer, C.-H. Yang, M. D. Rossell, Y.-H. C. P. Yu, J. F. Scott, J. W. A. III, L. W. Martin, et al., Nature Nanotechnology **5** (2010).

<sup>5</sup> J. Seidel, L. W. Martin, Q. He, Q. Zhan, Y.-H. Chu, A. Rother,

- M. Hawkridge, P. Maksymovych, P. Yu, M. Gajek, et al., Nat. Mater. **8**, 229 (2009).
- <sup>6</sup> A. Lubk, S. Gemming, and N. Spaldin, Phys. Rev. B **80**, 104110 (2009).
- <sup>7</sup> Y.-W. Chen, J.-L. Kuo, and K.-H. Chew, J. Appl. Phys. **122**, 075103 (2017).
- <sup>8</sup> O. Diéguez, P. Aguado-Puente, J. Junquera, and J. Íñiguez, Phys. Rev. B **87**, 024102 (2013).
- <sup>9</sup> G. Kresse and J. Furthmüller, Comput. Mater. Sci. **6**, 15 (1996).
- <sup>10</sup> S. L. Dudarev, G. A. Botton, S. Y. Savrasov, C. J. Humphreys, and A. P. Sutton, Phys. Rev. B **57**, 1505 (1998), URL <https://link.aps.org/doi/10.1103/PhysRevB.57.1505>.
- <sup>11</sup> A. Jain, S. P. Ong, G. Hautier, W. Chen, W. D. Richards, S. Dacek, S. Cholia, D. Gunter, D. Skinner, G. Ceder, et al., APL Materials **1**, 011002 (2013), ISSN 2166532X, URL <http://link.aip.org/link/AMPADS/v1/i1/p011002/s1&Agg=doi>.
- <sup>12</sup> B. Meyer and D. Vanderbilt, Phys. Rev. B **65**, 104111 (2002).
- <sup>13</sup> M. Yang, A. Bhatnagar, and M. Alexe, Advanced Electronic Materials **1** (2015).
- <sup>14</sup> K. Momma and F. Izumi, Journal of Applied Crystallography **44**, 1272 (2011), URL <http://dx.doi.org/10.1107/S0021889811038970>.